Materials Chemistry and Physics 256 (2020) 123761

Contents lists available at ScienceDirect

Materials Chemistry and Physics

journal homepage: www.elsevier.com/locate/matchemphys

Solvent effects on structural changes in self-healing epoxy composites

Ivana Radovic [a,*], Aleksandar Stajcic [b], Andjela Radisavljevic [c], Filip Veljkovic [a], Maria Cebela [a], Vojislav V. Mitic [d,e], Vesna Radojevic [f]

[a] University of Belgrade, VINCA Institute of Nuclear Sciences - National Institute of the Republic of Serbia, Mike Petrovica Alasa 12-14, 11351, Vinca, Beograd, Serbia
[b] University of Belgrade, Center of Microelectronic Technologies, Institute of Chemistry, Technology and Metallurgy – National Institute of the Republic of Serbia, Studentski Trg 16, 11000, Beograd, Serbia
[c] University of Belgrade, Innovation Centre, Faculty of Technology and Metallurgy, Karnegijeva 4, 11120, Belgrade, Serbia
[d] Institute of Technical Sciences of SASA, Kneza Mihaila 35, 11000, Belgrade, Serbia
[e] University of Nis, Faculty of Electronic Engineering, Aleksandra Medvedeva 14, 18000, Nis, Serbia
[f] University of Belgrade, Faculty of Technology and Metallurgy, Karnegijeva 4, 11120, Belgrade, Serbia

HIGHLIGHTS

- Software analysis enabled estimation of the surface damaged by impact test.
- Residual solvent was found in the samples where toluene was used as a solvent for the catalyst.
- Structural changes were observed in Grubbs catalyst that could influence its catalytic activity.
- Filled hollow-glass capillaries acted as a reinforcement for a fiber-reinforced epoxy matrix.
- The system with dissolved healing agents enabled high recovery of the impact strength.

GRAPHICAL ABSTRACT

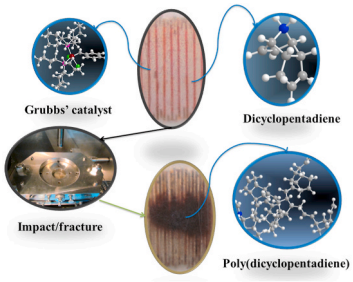

ARTICLE INFO

Keywords:
Self-healing
Solvent effect
Morphological properties
Structural investigation
Mechanical properties

ABSTRACT

Nowadays, there is a very high importance of composite research and variety of their applications in the modern world. In that sense, we researched hollow glass capillaries filled with dissolved Grubbs catalyst (GC) and dicyclopentadiene (DCPD) were incorporated into a fiber-reinforced epoxy with the aim of improving the flow of healing agents to the crack site. The morphological investigation of the crack site was performed using field emission scanning electron microscopy (FESEM), showing the difference between the samples depending on the used solvent. The software analysis of sample photographs has been performed by calculating the fractured/healed surface area of the samples, revealing that approximately 20% of the volume was affected by the impact. Fourier transform infrared spectroscopy (FTIR) revealed that poly (dicyclopentadiene) (PDCPD) formed at the healed interface. However, the FTIR investigation of catalyst stability in different solvents showed structural changes in GC and partial deactivation. The mechanical tests of the samples showed that a recovery of 60% after 24 h at room temperature could be achieved through the use of a solvent and very low concentration of GC. The performed research results are a good base to develop the model for predicting the processes and morphology, with the goal to design the final mechanical and in the future, thermal, properties in advance. This opens a new direction for future research in the field of composite healing.

* Corresponding author.
E-mail addresses: ivana_r@vinca.rs (I. Radovic), stajcic@nanosys.ihtm.bg.ac.rs (A. Stajcic), aradisavljevic@tmf.bg.ac.rs (A. Radisavljevic), vmitic.d2480@gmail.com (V.V. Mitic), vesnar@tmf.bg.ac.rs (V. Radojevic).

https://doi.org/10.1016/j.matchemphys.2020.123761
Received 18 May 2020; Received in revised form 28 July 2020; Accepted 21 August 2020
Available online 27 August 2020

1. Introduction

The self-healing ability of polymer-based materials has been recognized as an important field for research due to a potential prolongation of materials work time and the avoidance of catastrophic failure, characteristic of polymeric materials [1–4]. Over the years, materials with different self-healing mechanisms have been proposed and investigated [5]. Today, there are a number of materials with healing ability, some of them being able to heal without interventions like high temperature, UV, etc. (autonomous), and some of them needing initiation (non-autonomous) [6–8]. They can also be classified as presented on Scheme 1, the extrinsic ones have a system implemented in the structure, while the intrinsic ones have a structure that enables self-healing [9–16]. Common classification of self-healing mechanisms is given on Scheme 1.

Autonomous systems are developed without the use any external stimulus, which is a very relevant advantage. Intrinsic systems, although attractive due to their structural ability to promote self-healing, usually require external stimulus (non-autonomous) or have a low healing efficiency [17]. Extrinsic systems are usually autonomous; however, despite the very interesting self-healing behavior, these systems are very expensive due to the impossibility to use the ruthenium catalyst in a low amount (as catalyst dispersed in the form of molecular complex in the matrix). Among the materials with extrinsic healing systems, composites with an epoxy matrix are the most studied so far because of their good mechanical and chemical properties, and a wide field of application, especially in the aeronautical and automotive industry, where the material is exposed to a strong mechanical tension and there is a probability of puncture [18–23]. The epoxy matrix is usually reinforced with glass or carbon fibers, which contribute significantly to the mechanical strength of the composite [24–30]. However, fiber-reinforced composites are also prone to the formation of microcracks that cause material failure. This challenge could be resolved through self-healing if liquid healing agents would flow efficiently into cracks, allowing a chemical reaction to take place, thus building an adhesive for the damaged composite. As many other findings in science, the self-healing of materials is based on natural processes, like bone or wound healing. As can be seen on Scheme 1, one candidate for storing the liquid healing agents is the hollow fiber/capillary. One of the first implemented systems consisted of large hollow capillaries filled with monomer dicyclopentadiene (DCPD), while the first generation Grubbs catalysts (GC) was spread all over the epoxy matrix [31,32]. The self-healing systems have also been improved and changed in the direction of polymeric micro/-nanocapsules filled with monomer where a small, insufficient amount of healing agents is being used [33–40]. In the case of the catalyst particles embedded in the epoxy resin, the catalyst particles which are locally in contact with the oxirane rings (during the curing reactions) deactivate, hence reducing the actual amount of active catalyst [41]. Microencapsulation approach suffers from the great drawback related to the high cost of the catalyst (especially Grubbs and Hoveyda-Grubbs catalyst). However, to overcome this limitation, protected Ru-catalyst, immobilized on graphene sheets, through polymeric globular shell, was prepared and used for Ring Opening Metathesis Polymerization (ROMP) in strongly reactive environments based on epoxy resins. As a result, reduction from 5% to 0.3% by wt of expensive catalyst in the self-healing composite material was achieved [42]. Furthermore, in order to overcome the drawback related to the high cost of the catalyst, a new stable initiator for ROMP reactions, suitably designed to be embedded in structural resins, has been synthetized [43].

A uniform distribution of such small amounts of a catalyst at the crack site is also a challenge. The dissolution of GC could enable its flow to the healing site, provided that the applied solvent does not disrupt the activity of the catalyst or the overall properties of the matrix. With the proper selection of a moderately evaporative solvent, once the crack is formed, catalyst could easily flow to the healing site. Another important issue that needs to be resolved is choosing an appropriate container for the catalyst solution, which would crack and open with the composite, but not during the regular operation conditions. Glass capillaries could serve as good testing containers, having acceptable mechanical properties. They could even serve as reinforcement for the matrix. So far, hollow fibers have been employed as containers for the two-component epoxy resins that would replace matrix at the healing site [44,45]. Some researchers added color in order to follow the self-healing progress in the matrix [46]. Most of the researches used the fact that the hollow fibers can provide much higher amounts of healing agents compared to microcapsules and vascular networks. The results of recovered bending strength were up to 90%, but it has been established that the resin becomes less active over time. The direction of storing dissolved GC in the hollow glass capillaries for the use in the epoxy-reinforced composites has not been explored, although it could enable a researcher to conduct a visual inspection over the GC stability during composite processing as well as the use of a very low amount of the catalyst.

In this study, the epoxy-based matrix reinforced with fiberglass mat was used with embedded filled glass capillaries. The solvents used for GC were dichloromethane (DCM) and toluene (TO), commonly used solvents for dissolution of GC. Therefore, the catalyst is expected to remain stable in named solvents during processing and exploitation. DCPD was used as a monomer, mixed with N, N′-dimethylformamide (DMF). The influence of the solvents on GC stability and healing ability as well as the influence of filled capillaries on the mechanical properties of the virgin (undamaged) material were investigated. In this manner,

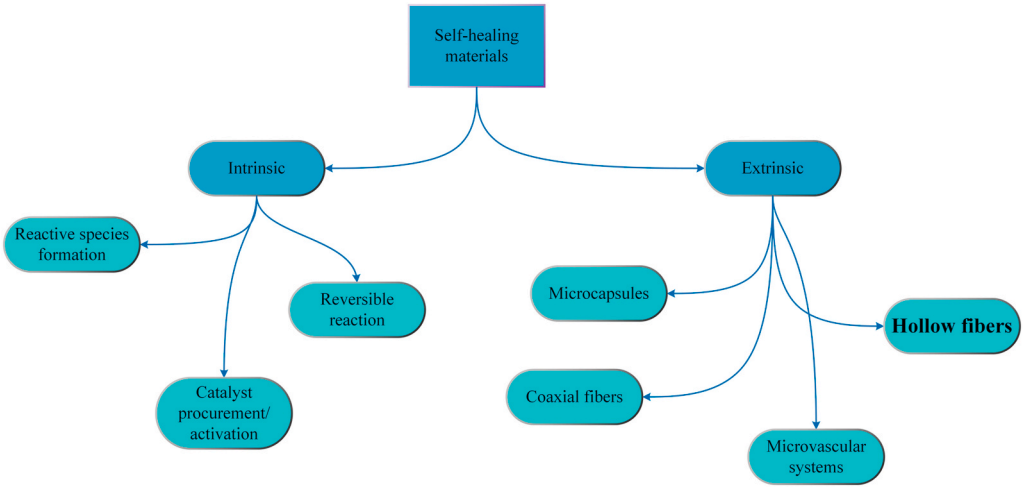

Scheme 1. Classification of self-healing mechanisms.

flow of the catalyst using solution could be investigated and further research on the development of smaller containers will be performed.

2. Experimental

2.1. Materials and methods

The first-generation Grubbs catalyst (GC), dimethylformamide 99.8% (DMF), dichloromethane (DCM), and toluene (TO) were purchased from Sigma-Aldrich. Dicyclopentadiene (DCPD) was obtained from Acros Organics. Bisphenol A diglycidyl ether (DGEBA)-based epoxy resin and diethylenetriamine (DETA)-based hardener were purchased from R&G Faserverbundwerkstoffe GmbH, Composite Technology, Waldenbuch. The fiberglass mat was the reused material from Izolma, Raca, treated with urea for the previous use.

The glass capillaries (with the inner diameter of 1.35 mm and the length of 50 mm) were filled with two types of different solutions. The first type of solution was 10 wt% DCPD in DMF. Another type of solution was 1 wt % solution of GC in different solvents, DCM and TO. The ends of the capillaries were clogged with plasticine, which prevented leaking of the solution. All solvents were selected using a map of the Hansen solubility parameters, as well as recommendations for maintaining catalyst stability.

The epoxy resin and the DETA-based hardener were mixed in a volume ratio of 20:9, following the manufacturer's procedure. Vigorous mixing of the epoxy precursor and the crosslinker, to ensure optimal crosslinking at room temperature, lasted for 2 min. Immediately after mixing the epoxy resin and the hardener, eight layers of the non-woven fiberglass mat (5.8 wt % in the composite) were soaked in the mixture. The composite was left in a silicone mold during 24 h in order for the resin to crosslink in the presence of the hardener. A series of samples containing only the matrix and the fiberglass mats was denoted as a control group 0 (C0). Control group 1 (denoted as C1) contained only the DCPD/DMF-filled glass capillaries in the epoxy-fiberglass composite. The composite with the glass capillaries alternately filled with the GC/DCM and the DCPD/DMF solutions was denoted as GCDCM, while composite with the glass capillaries alternately filled with the GC/TO and the DCPD/DMF solutions was labeled as GCTO. The concentrations of GC and DCPD in all of the samples are given in Table 1. All of the capillaries were inserted in the middle of the composite samples, between the fourth and the fifth layer of the fiberglass mat; the thickness of the samples being 7 mm.

The three-dimensional model of an enlarged layer of processed composites with alternately-arranged catalyst (purple) and monomer (gray) solutions is shown in Fig. 1.

2.2. Characterization of the samples

In order to determine the morphology of the fiberglass and the fracture site, each processed composite was monitored using Field Emission Scanning Electron Microscope (FESEM) (JSM 5800, Tescan Mira 3). Micrographs have been analyzed in the program *Image-Pro Plus*. FTIR was performed for the investigation of GC stability in DCM and TO as well as for the identification of polymerized DCPD and comparison with the starting components. All of the samples (C0, C1, GCDCM, and GCTO which were crushed into a powder) were mixed with KBr and the resulting powders were compressed into tablets for infrared testing.

Table 1
Formulations of prepared composite samples with glass capillaries.

Sample	Concentration GC, wt%	Concentration DCPD, wt%
C0	0	0
C1	0	1.04
GCDCM	0.035	0.52
GCTO	0.035	0.52

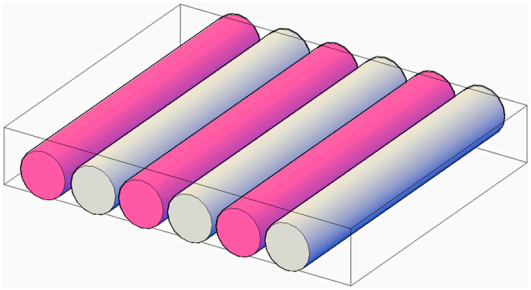

Fig. 1. 3D model of the enlarged cross-section of the composite layer.

FTIR spectra in the range of 4000–400 cm^{-1} were recorded using a FTIR spectrometer (BOMEM Michelfan MB-102 FTIR). In order to investigate self-healing efficiency, a controlled-energy impact test was performed. Healing efficiency, η (defined as the ability to recover a sample after the impact), was determined from the impact analysis based on the following equation:

$$\eta = E_{healed}/E_{virgin} * 100\% \quad (1)$$

where E_{virgin} and E_{healed} represent the absorbed energies (energy at maximum load, E_{fmax}, or total absorbed energy, E_{tot}) of the samples during the first impact and after the healing, respectively.

3. Results and discussion

3.1. Visual analysis of damage site digital photographs

Photographs of the GCDCM and GCTO samples before the impact can be seen in Fig. 2. The images of GCDCM show the GC-solution change in color in some places, from purple (the original solution color) to yellow and brown, implying a partial loss of its activity during processing, which is in accordance with FTIR findings. This color change is neglectable in GCTO, which means it kept stability during the filling of the capilaries and further processing of the composites.

The advantage of the filled glass capillary system is the visual inspection of damage as well as healing at the fracture site. Fig. 3 shows the front and back side of the GCDCM and GCTO after the healing. The fracture area can be seen after the healing, showing a dark-colored area covered by the formed poly (dicyclopentadiene) PDCPD.

The photographs show the successful inflow of the GC and DCPD

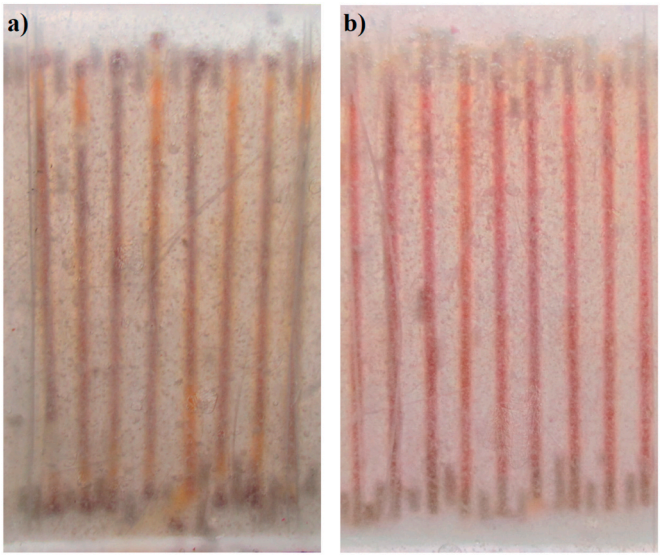

Fig. 2. a) GCDCM and b) GCTO before the impact.

solutions to the crack. At the back of the GCDCM and GCTO samples, the separation of the matrix along the crack border can be seen, caused by the cracking of the glass capillaries. Using the image-analysis software *Image-Pro Plus*, the approximate damaged surface area covered by the formed PDCPD was calculated. The front and the back side masks of the healed samples (Fig. 4) show the surface that software automatically calculates as a given object.

All the samples had the surfaces of 36 cm^2 (6 × 6 cm^2). The front side of the newly-formed polymer coverage GCDCM sample was approximately 7.34 cm^2 or 20.4% of the total sample area, while the coverage of the back side was 9.88 cm^2 or 27.5% of the total surface area. For the GCTO sample, the coverage is approximately 23.0% of the surface viewed from the front and 21.7% from the back. Considering the estimated fraction of the healed crack, a considerable difference in the absorbed energy was expected between the samples with the healing agents and the control samples.

3.2. Morphological analysis of fractured composite samples

Residual solvent, presumably toluene, was found at the crack site in the GCTO samples (Fig. 5). Obviously, a portion of the low-evaporating solvent could not be removed in time before the sealing of the crack and it remained trapped inside the healed composite. Ability to observe such phenomena is one of the advantages of using filled glass capillaries.

Different effects of the residual solvent in the composites have been reported, some of them including mechanical strength enhancement induced by the residual *N*,*N*-dimethylformamide or filling of the voids by *N*,*N*-Dimethylacetamide and Nmethyl-2-pyrrolidone [47,48]. Formation of solvent drops in GCTO fracture site gives direction for further study of a residual solvent with high boiling temperature and its influence on the healing ability and mechanical properties of the composite.

3.3. FTIR spectroscopy

3.3.1. FTIR analysis of GC stability in solvents

Infrared spectroscopy of the GC solutions in DCM and TO showed structural changes in GC caused by the exposure to DCM. The spectra obtained by the analysis are shown in Figs. 6 and 7. In order to emphasize the differences between spectra, the range of 4000 to 400 cm^{-1} was split into four regions:

1) The region of 4000-2000 cm^{-1}, where all three spectra have identical bands, coming from the –OH and –CH stretching (Fig. 6a): a relatively broad band around 3440 cm^{-1}, coming from hydrogen bonded hydroxyl groups, points to moisture absorption during sample preparation for FTIR measurements, or even during the catalyst dissolution [49].

A peak at 3055 cm^{-1}, from the aromatic benzene ring asymmetric C–H bond stretching appeared in all three spectra. In GC/TO spectrum, toluene gives contribution to this band as well as GC [50]. Asymmetric and symmetric –CH stretching from aliphatic $–CH_2$ and $–CH_3$ was visible around 2920 cm^{-1} and 2850 cm^{-1}, respectively [51,52]. These high intensity bands were noticeable in all three spectra, coming from GC, DCM, and TO.

2) *The region of 2000*-850 cm^{-1}, where most of the bands originate from aromatic ring bonds, with the exception of GCDCM, which showed unexpected possible structural change (Fig. 6b): in the GC/DCM two unexpected peaks emerged, at 1934 cm^{-1} and 1890 cm^{-1}, both indicating the formation of a carbonylated Ru complex. The first band corresponds to Ru–CO, while the second probably comes from bridged –CO [53–55].

The reason for such decomposition of GC is the presence of oxygen in glassware, catalyst, or solvents [56]. The partial change in color of the GC/DCM solution into yellow and dark brown, observed on photographs, is consistent with this discovery. Although this reaction can happen in toluene as well, in this case, GC remained intact in TO during the same processing conditions as in DCM. The increased GC susceptibility to degradation in DCM is probably caused by a higher DCM polarity compared to. The GC/TO spectrum showed two strong C–C stretches of the aromatic ring at 1606.5 cm^{-1} and 1508.9 cm^{-1}, due to a dominant presence of TO [57]. A peak that appeared at 1445 cm^{-1} came from the bending of the sp^3 hybridized carbon C–H bonds. In the GC/DCM spectrum, a $–CH_2$ deformation from DCM was observed. The bands at 1244, 1173, and 1151 cm^{-1} come from the –CCH deformation and ring stretching [58]. An in-plane –CH bending was present at 1075, 1044, and 1005 cm^{-1}. At 933 cm^{-1} small, sharp peak from a –CH out-of-plane deformation can be seen on GC GC/TO but is missing on GC/DCM. Most of the bands in the region from 900 cm^{-1} to 650 cm^{-1} come from the aromatic ring –CH out-of-plane bending [59,60]. At 896 cm^{-1}, a vinylidene –CH out-of-plane bending peak shape change is evident in GC/DCM, compared to GC and GCTO, which could be caused by the loss of –C═C bond between Ru and Ph during the partial decomposition of GC [56].

3) *The region of 850*-650 cm^{-1}, where the differences in aromatic peaks between GC/DCM and the other two samples are pronounced (Fig. 7a): in GCTO, an additional broad band of –CH out-of-plane bending appeared at 827 cm^{-1}. Both GC and GCTO expressed the –CH out-of-plane bending from monosubstitued aromatic at 750 cm^{-1}, while a shift towards a lower frequency, 740 cm^{-1}, can be seen in GC/DCM spectrum. Next to that, two sharp –CH out-of-plane bending peaks, at 736 cm^{-1} and 730 cm^{-1}, appeared in the GC and GC/TO spectra; in GC/DCM, a mild shoulder is visible at 738

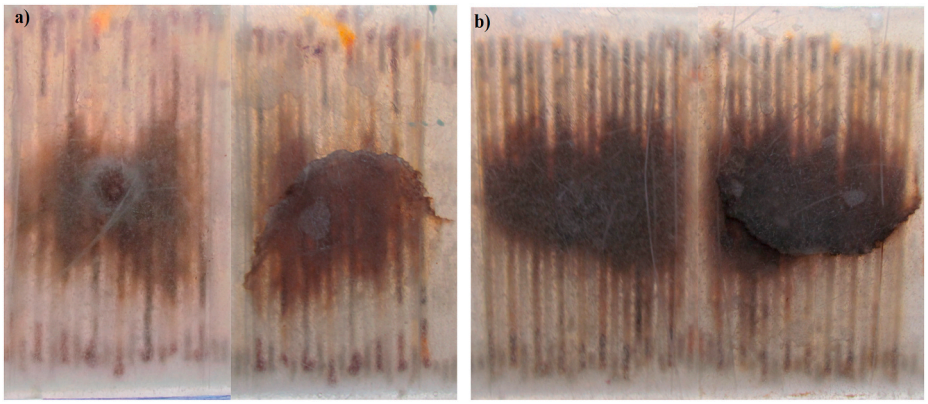

Fig. 3. Damaged zone, front (left) and back (right) side 24 h after the impact of.

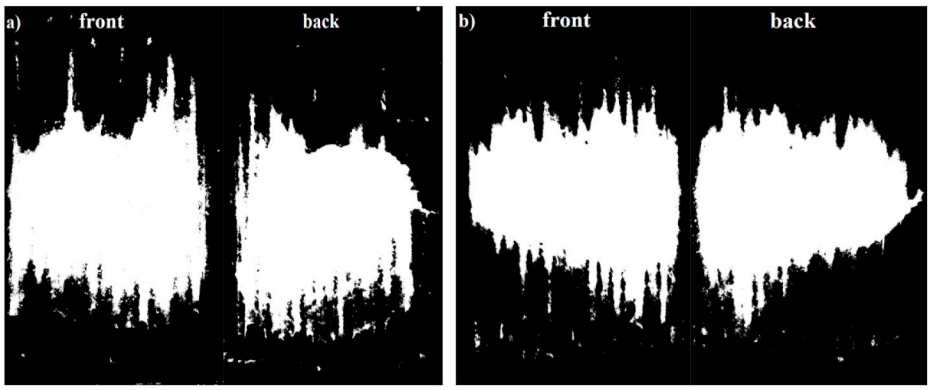

Fig. 4. Front (left) and back (right) side masks of: a) GCDCM; b) GCTO.

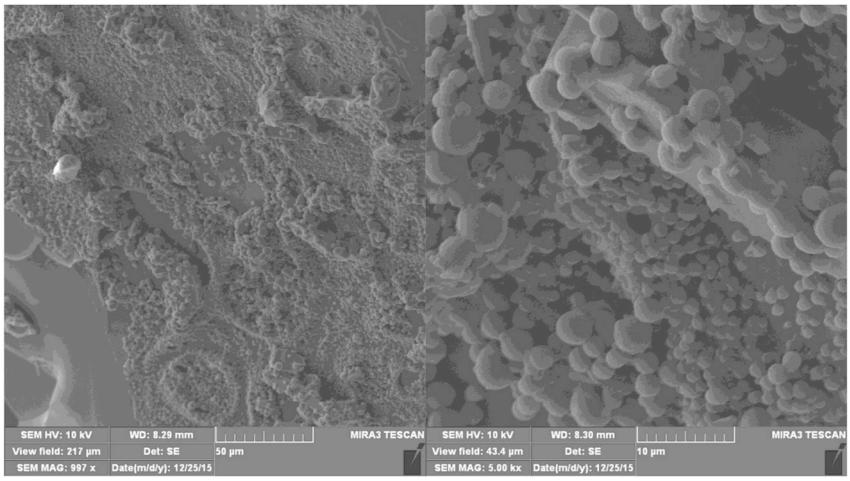

Fig. 5. Residual solvent in GCTO.

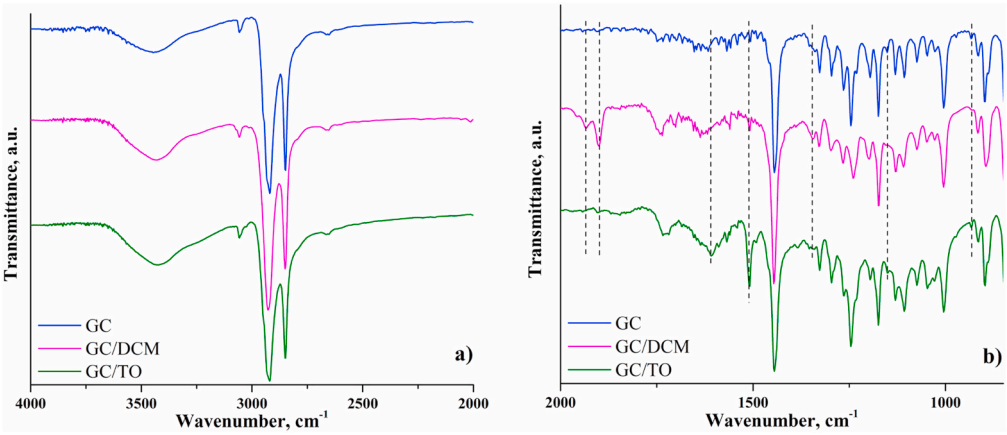

Fig. 6. FTIR spectra of GC, GC/DCM and GC/TO: a) Region 4000-2000 cm^{-1}; b) Region 2000-850 cm^{-1}.

cm^{-1}. All of these shifts and shape changes in peaks indicate different surrounding groups around phenyl in GC, as a consequence of partial structural change in DCM caused by the contact with oxygen.

4) *The region of 650-400* cm^{-1}, where one the most important peaks in GC has been identified as well as its shape differences between GC in DCM and the rest of GC (Fig. 7b): in the GC/DCM spectrum, the peak originating from the asymmetric C–Cl stretching from DCM appears at 648 cm^{-1}. At 521 cm^{-1}, GC and GC/TO have exhibited a medium sharp peak that originates from the Ru–P bond, which in GC/DCM appeared as a shoulder followed by a stronger peak at 510 cm^{-1}, present in all three spectra [61]. Ru–P is the most commonly broken bond during deactivation of GC. Its preservation, along with other characteristic GC bonds indicates that GC remained in its active form in TO. The diminished peak in GC/DCM means that the activity is not lost but only reduced due to a partial deactivation. This can also be observed on impact images, where only parts of the catalyst solution changed in color to yellow and brown.

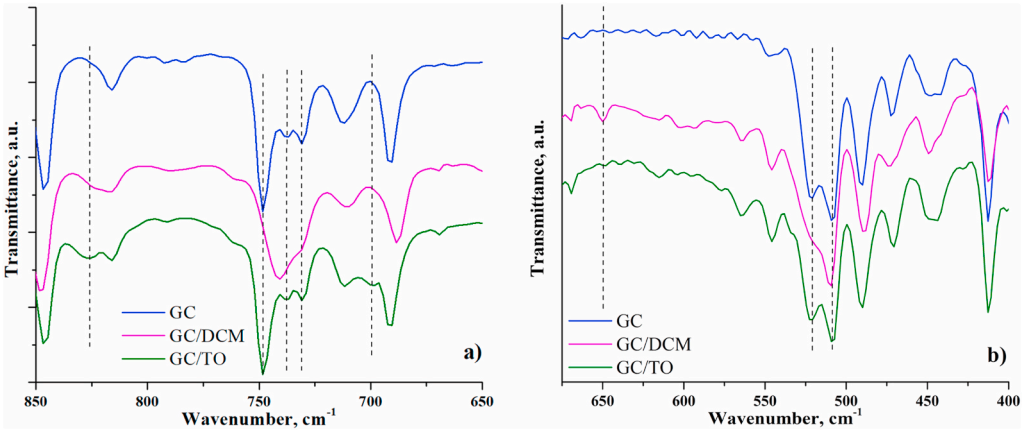

Fig. 7. FTIR spectra of GC, GC/DCM and GC/TO: a) Region 850-650 cm^{-1}; b) Region 650-400 cm^{-1}.

3.3.2. *FTIR analysis of composite fracture*

The spectra of DCPD and epoxy-fiberglass mat (C0) fracture site were compared with the GCDCM and the GCTO healed fracture sites (Fig. 10) in order to establish whether the polymerization of DCPD was successful in the presence of GC solutions. The reaction of epoxide crosslinking is presented in Fig. 8.

Fig. 9 shows a presumed reaction of DCPD ring opening metathesis polymerization (ROMP) in the presence of GC. Being that the first generation Grubbs catalyst used in this study shows high selectivity, the only expected product was *trans*-PDCPD [62].

In the spectrum of C0, the C–C–O–C symmetric stretch from DGEBA appeared around 1181 cm^{-1}. The GCDCM and GCTO healed sites spectra did not show this band, neither did C–N stretching around 1115 cm^{-1} [63]. Additionally, C0 was the only spectrum showing the aromatic –CH in-plane bending at 1110 and 1035 cm^{-1} and the –CH out-of-plane bending at 827 cm^{-1}. All of these differences between the C0 and other spectra indicate that the randomly sampled material from healed sites did not contain epoxy matrix. The DCPD bands in the region from 1000 to 600 cm^{-1} are mostly associated with the –CH out-of-plane bending. Around 676 cm^{-1}, the –CH bending from the *cis*-cyclic double bond of the cyclopentene ring appeared in the DCPD and GCDCM spectra, while it was slightly shifted to 670 cm^{-1} in GCTO [63,64]. The peak intensity drop is obvious between GCDCM and GCTO, which could be the consequence of a higher crosslinking degree in GCTO. The

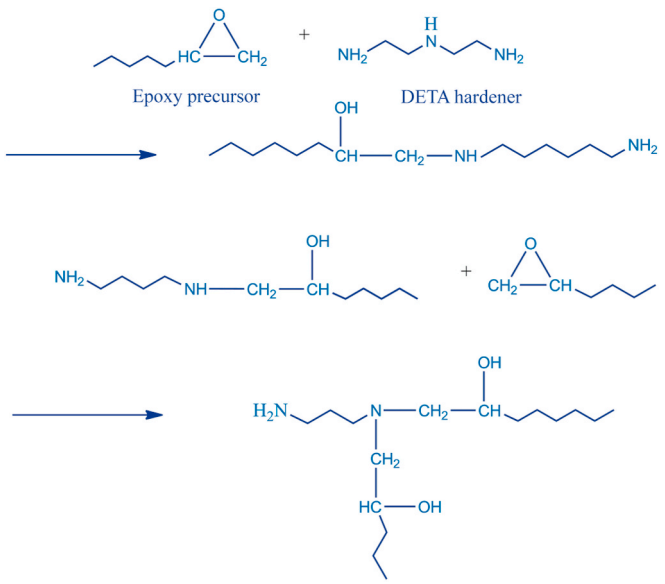

Fig. 8. Formation of epoxy matrix.

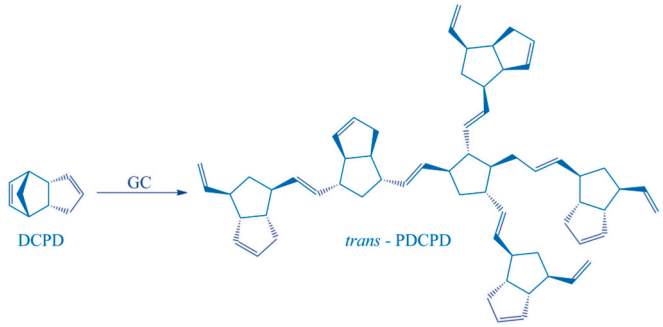

Fig. 9. ROMP of DCPD catalyzed by GC.

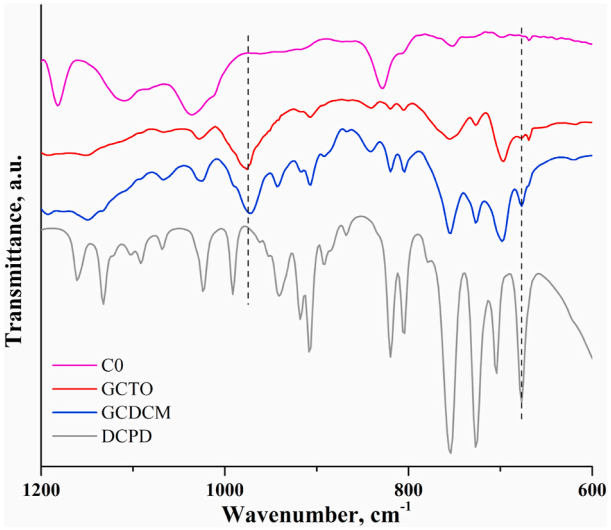

Fig. 10. FTIR spectra of the C0, GCDCM, and GCTO fracture sites and the liquid monomer DCPD.

trans-double bond of the open, polymerized, DCPD ring was identified with the –CH out-of-plane bending at 973 cm^{-1} in both GCDCM and GCTO [64–67]. Being that the concentrations of GC and DCPD have been very low in the composite samples, the intensity of the peaks and the missing high-intensity bands from the used solvents (DCM, TO, DMF) led to a conclusion that the solvents have mostly evaporated from the fracture surface, although the FESEM images show residual solvent in GCTO. Obviously, the solvent has not been captured during the sampling of FTIR measurement being that it was observed only in one

region of the FESEM sample.

3.4. Controlled energy impact test

The shape of the load-time curves obtained by a controlled energy impact test showed a ductile fracture for all the virgin samples (Fig. 11), which is expected because the samples were not exposed to a subsequent crosslinking of epoxy at high temperatures after 24 h at room temperature in order to avoid the boiling of DCM and the deactivation of GC.

After the second impact, the control sample C0 (a composite epoxy-fiberglass mat) showed ductile-brittle fracture (Fig. 11a), which is a direct consequence of the resulting crack that contributes to the destruction of the sample upon the second impact. A C0 virgin absorbs a lower amount of energy (Fig. 12) compared to C1 (the composite epoxy-fiberglass mat with DCPD/DMF glass capillaries), indicating that the filled capillaries have the role of reinforcement in a composite material, which was already confirmed in previous studies, where they used different filling agents in epoxy and tested bending strength [46]. However, after the first impact, a larger crack and the separation of the matrix along the brim of the crack were created in the sample C1 compared to C0, due to the fractured capillaries break on the sample surface. As a consequence, C1 had reduced ability to absorb energy during the second impact (Fig. 12). Also, the transition from a ductile to a brittle fracture is a direct consequence of an existing crack that expands and leads to a sudden, catastrophic fracture (Fig. 11a). GCDCM retains ductile behavior (Fig. 11b), indicating that DCPD is not fully crosslinked [68]. The degree of crosslinking can be increased by the exposure to high temperatures, where self-healing efficiency would probably increase, but the system would lose autonomy which was not the goal of this research. The GCTO sample exhibits a more brittle fracture during the first impact and retains this type of fracture during the second impact, due to an influence of PDCPD with higher degree of crosslinking that was indicated in the FTIR analysis with a low-intensity band for the *cis*-cyclic double bond of the cyclopentene ring. The other factor that could influence healed GCTO curve shape is the unfilled crack volume at the healing site.

Fig. 12 illustrates changes in absorbed energy at the maximum load (E_{fmax}) and the total absorbed energy (E_{tot}) where the former represents energy absorbed until the damage initiation and failing and the latter stands for the energy absorbed during the complete test [69]. In the case of a sudden failure, characteristic of brittle materials E_{fmax} and E_{tot} can be equal. The difference between the two can indicate the type of a fracture.

Both virgin GCDCM (4.51 J) and GCTO (4.43 J) absorbed a higher amount of energy (E_{tot}) than C0 (4.03 J), which confirms the reinforcing effect of the filled capillaries seen in C1 (Fig. 12a). After being placed to heal for 24 h in a room temperature-adjusted chamber (25 °C), healed GCDCM and GCTO absorbed around 2.5 times more energy than C0, and around 4 times more than C1. The E_{tot} values indicate that, despite the separation of the matrix by capillary eruption, a high percentage of the initial impact strength can be recovered by healing. GCDCM showed 60%, while GCTO exhibited 51% of the E_{tot} recovery. With only 0.035 wt% of the catalyst, up to 60% of recovery was achieved, which can be considered as very high-healing efficiency.

The E_{fmax} values revealed an interesting behavior of GCTO. Namely, its highest value (4.20 J) shows that it can absorb more energy compared to other samples before the crack initiation and can be considered the toughest. Furthermore, after the healing, recovery of E_{fmax} is over 53%, while GCDCM showed 47.5%, which means that the healed GCTO has the highest E_{fmax} among all of the damaged samples. The close values of E_{fmax} and E_{tot} for GCTO healed indicate a brittle fracture which is expected based on the assumption from FTIR and shape of impact test curves – higher degree of crosslinking of DCPD was achieved compared to the fracture site of GCDCM.

All of these results and analyses give us the new research opportunities for processing, morphology and structural changes by effected by a variety of solvents. In composites investigated, the fractures appearing play very important role on the structural integrity. Therefore, we consider extending further research towards the application of fractal nature analysis within the fractures.

4. Conclusion

This study provides insight in the solvent influence on the Grubbs catalyst (GC) stability and the composite healing ability. The system of filled glass capillaries was used for the healing agent delivery and the additional reinforcement of the fiber-reinforced epoxy matrix. In order to ensure the stability of the catalyst during processing, it was dissolved in the most commonly used solvents for synthesis involving GC – toluene and dichloromethane. A morphological investigation showed a residual high-boiling temperature solvent at the fracture site of the GCTO sample which could influence mechanical and healing behavior of the composite. On the other hand, an infrared spectroscopy analysis showed two unexpected peaks in the spectrum of the GC/DCM solution, both indicating formation of the carbonylated Ru complex due to the presence of oxygen in the working environment. These peaks, along with the loss of different aromatic bands were supported by a change in color, from purple to yellow and brown, in a few of the capillaries which proves a partial deactivation of GC. The formation of a poly (dicyclopentadiene) (PDCPD) was confirmed with a *trans*-double bond of a polymerized DCPD ring in both GCDCM and GCTO. The C*is*-cyclic double bond peak intensity difference between GCDCM and GCTO indicates a higher crosslinking degree in GCTO which leads to a more brittle mechanical behavior. The controlled energy impact test showed that the filled

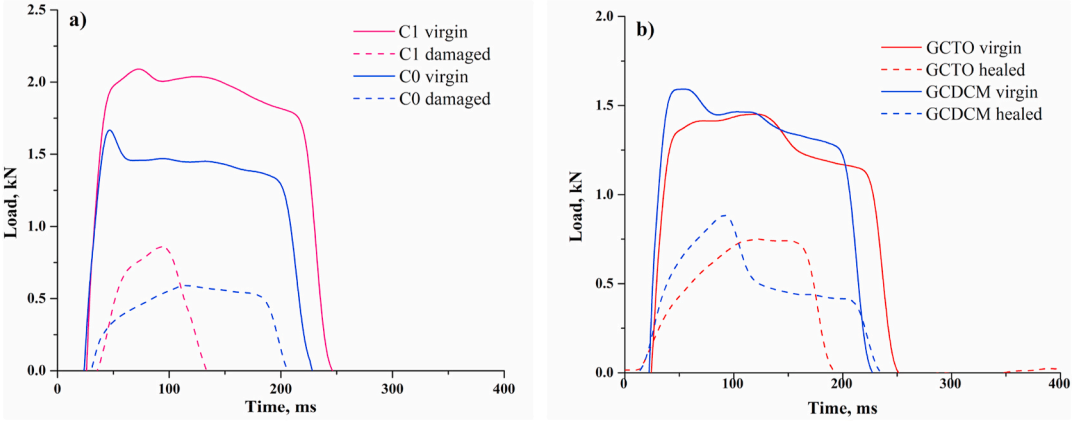

Fig. 11. Impact test load-time curves for: a) C0 and C1; b) GCTO and GCDCM.

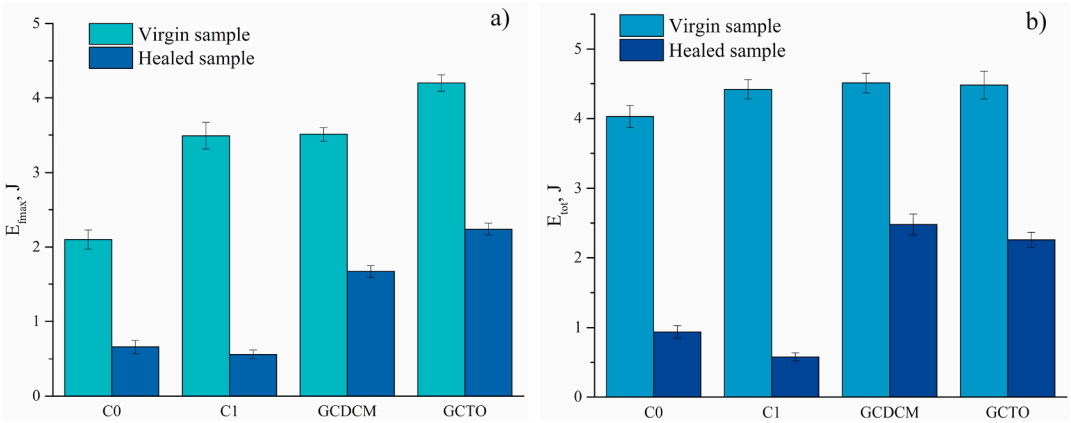

Fig. 12. Values of: a) E_{fmax}; b) E_{tot}.

capillaries serve as reinforcement for the composite during the initial stroke. After the 24 h-healing at room temperature, GCDCM kept ductile fracture which is in accordance with the infrared spectroscopy finding of a low DCPD crosslinking degree at the healing site. On the other hand, due to a higher crosslinking degree, the healed GCTO sample exhibited more brittle behavior. The total absorbed energy values (E_{tot}) showed that with only 0.035 wt% of GC in the samples, a satisfactory percentage of the initial impact strength can be recovered by healing: GCDCM showed 60%, while GCTO exhibited 51% recovery. Energy at the maximum load (E_{fmax}) provided new insight in the GCTO behavior, which was able to absorb the highest amount of energy before the damage initiation, thus opening the door for further investigation into the reinforcing influence of the residual solvent potential. All of the findings in this research show that the system with solutions of GC should be further explored being that they can potentially offer high healing efficiency along with interesting scientific phenomena. These research results also open the new frontiers in predicting the composite structures by solvent influence.

Funding

This work was financially supported by the Ministry of Education, Science and Technological Development of the Republic of Serbia (Grant No. 451-03-68/2020–14/200017 and 451-03-68/2020–14/200026).

CRediT authorship contribution statement

Ivana Radovic: Conceptualization, Writing - original draft, Methodology, Formal analysis. **Aleksandar Stajcic:** Writing - original draft, Formal analysis. **Andjela Radisavljevic:** Investigation. **Filip Veljkovic:** Data curation, Visualization. **Maria Cebela:** Formal analysis. **Vojislav V. Mitic:** Supervision. **Vesna Radojevic:** Funding acquisition.

Declaration of competing interest

The authors declare that they have no known competing financial interests or personal relationships that could have appeared to influence the work reported in this paper.

References

[1] M.Q. Zhang, M.Z. Rong, Self-healing Polymers and Polymer Composites, Hoboken, New Jersey, 2011.
[2] M. Nosonovsky, B. Bhushan, Surface self-organization: from wear to self-healing in biological and technical surfaces, Appl. Surf. Sci. 256 (2010) 3982–3987, https://doi.org/10.1016/j.apsusc.2010.01.061.
[3] C.E. Diesendruck, N.R. Sottos, J.S. Moore, S.R. White, Biomimetic self-healing, Angew. Chem. Int. Ed. 54 (2015) 10428–10447, https://doi.org/10.1002/anie.201500484.
[4] V.K. Thakur, M.R. Kessler, Self-healing polymer nanocomposite materials: a review, Polymer 69 (2015) 369–383, https://doi.org/10.1016/j.polymer.2015.04.086.
[5] N.J. Kanu, E. Gupta, U.K. Vates, G.K. Singh, Self-healing composites: a state-of-the-art review, Compos. Part A Appl. Sci. Manuf. 121 (2019) 474–486, https://doi.org/10.1016/j.compositesa.2019.04.012.
[6] B. Willocq, R.K. Bose, F. Khelifa, S.J. Garcia, P. Dubois, J.M. Raquez, Healing by the Joule effect of electrically conductive poly(ester-urethane)/carbon nanotube nanocomposites, J. Mater. Chem. A. 4 (2016) 4089–4097, https://doi.org/10.1039/c5ta09793b.
[7] H.B. Yue, J.P. Fernández-Blázquez, D.F. Beneito, J.J. Vilatela, Real time monitoring of click chemistry self-healing in polymer composites, J. Mater. Chem. A. 2 (2014) 3881–3887, https://doi.org/10.1039/c3ta14961g.
[8] Y. Xu, D. Chen, Self-healing polyurethane/attapulgite nanocomposites based on disulfide bonds and shape memory effect, Mater. Chem. Phys. 195 (2017) 40–48, https://doi.org/10.1016/j.matchemphys.2017.04.007.
[9] F. Verstraeten, R. Göstl, R.P. Sijbesma, Stress-induced colouration and crosslinking of polymeric materials by mechanochemical formation of triphenylimidazolyl radicals, Chem. Commun. 52 (2016) 8608–8611, https://doi.org/10.1039/c6cc04312g.
[10] M.A. Rhaman, M. Penco, G. Spagnoli, A.M. Grande, L. Di Landro, Self-healing behavior of blends based on ionomers with ethylene/vinyl alcohol copolymer or epoxidized natural rubber, Macromol. Mater. Eng. 296 (2011) 1119–1127, https://doi.org/10.1002/mame.201100056.
[11] L. Huang, N. Yi, Y. Wu, Y. Zhang, Q. Zhang, Y. Huang, Y. Ma, Y. Chen, Multichannel and repeatable self-healing of mechanical enhanced graphene-thermoplastic polyurethane composites, Adv. Mater. 25 (2013) 2224–2228, https://doi.org/10.1002/adma.201204768.
[12] V. Blanco, D.A. Leigh, V. Marcos, Artificial switchable catalysts, Chem. Soc. Rev. 44 (2015) 5341–5370, https://doi.org/10.1039/c5cs00096c.
[13] K. Pingkarawat, C.H. Wang, R.J. Varley, A.P. Mouritz, Self-healing of delamination cracks in mendable epoxy matrix laminates using poly[ethylene-co-(methacrylic acid)] thermoplastic, Compos. Part A Appl. Sci. Manuf. 43 (2012) 1301–1307, https://doi.org/10.1016/j.compositesa.2012.03.010.
[14] K. Pingkarawat, C.H. Wang, R.J. Varley, A.P. Mouritz, Mechanical properties of mendable composites containing self-healing thermoplastic agents, Compos. Part A Appl.Sci. Manuf. 65 (2014) 10–18, https://doi.org/10.1016/j.compositesa.2014.05.015.
[15] M. Nakahata, S. Mori, Y. Takashima, H. Yamaguchi, A. Harada, Self-healing materials formed by cross-linked polyrotaxanes with reversible bonds, Inside Chem. 1 (2016) 766–775, https://doi.org/10.1016/j.chempr.2016.09.013.
[16] D.Y. Zhu, M.Z. Rong, M.Q. Zhang, Self-healing polymeric materials based on microencapsulated healing agents: from design to preparation, Prog. Polym. Sci. 49–50 (2015) 175–220, https://doi.org/10.1016/j.progpolymsci.2015.07.002.
[17] L. Guadagno, L. Vertuccio, C. Naddeo, E. Calabrese, G. Barra, M. Raimondo, A. Sorrentino, W.H. Binder, P. Michael, S. Rana, Reversible self-healing carbon-based nanocomposites for structural applications, Polymers 11 (2019) 903.
[18] G. Li, O. Ajisafe, H. Meng, Effect of strain hardening of shape memory polymer fibers on healing efficiency of thermosetting polymer composites, Polymer 54 (2013) 920–928, https://doi.org/10.1016/j.polymer.2012.12.046.
[19] P.J. Halley, Morphology development in thermoset nanocomposites, in: V. Mittal (Ed.), Optimization of Polymer Nanocomposite Properties, Wiley-VCH Verlag GmbH & Co. KgaA, Weinheim, 2010, pp. 21–40.
[20] S. Kalia, S.Y. Fu, Polymers at Cryogenic Temperatures, Springer, Berlin, Heidelberg, 2013.
[21] L. Jesheng, W. Saopeng, S. Huang, P. Cong, P.M. Yixuan, Preparation of epoxy modified polysiloxane microemulsions, Iran. Polym. J. (Engl. Ed.) 18 (2009) 159–166.
[22] A.H. Korayem, M.R. Barati, G.P. Simon, X.L. Zhao, W.H. Duan, Reinforcing brittle and ductile epoxy matrices using carbon nanotubes masterbatch, Compos. Part A Appl. Sci. Manuf. 61 (2014) 126–133, https://doi.org/10.1016/j.compositesa.2014.02.016.

[23] G. Kickelbick, Introduction to hybrid materials, in: G. Kickelbick (Ed.), Hybrid Materials Synthesis, Characterization, and Applications, Wiley-VCH Verlag GmbH & Co. KgaA, Weinheim, 2007, pp. 1–48.
[24] F. Ellyin, R. Maser, Environmental effects on the mechanical properties of glass-fiber epoxy composite tubular specimens, Compos. Sci. Technol. 64 (2004) 1863–1874, https://doi.org/10.1016/j.compscitech.2004.01.017.
[25] J.G. Kim, I. Choi, D.G. Lee, I.S. Seo, Flame and silane treatments for improving the adhesive bonding characteristics of aramid/epoxy composites, Compos. Struct. 93 (2011) 2696–2705, https://doi.org/10.1016/j.compstruct.2011.06.002.
[26] K. Hargou, K. Pingkarawat, A.P. Mouritz, C.H. Wang, Ultrasonic activation of mendable polymer for self-healing carbon-epoxy laminates, Compos. B Eng. 45 (2013) 1031–1039, https://doi.org/10.1016/j.compositesb.2012.07.016.
[27] T. Yin, M.Z. Rong, J. Wu, H. Chen, M.Q. Zhang, Healing of impact damage in woven glass fabric reinforced epoxy composites, Compos. Part A Appl. Sci. Manuf. 39 (2008) 1479–1487, https://doi.org/10.1016/j.compositesa.2008.05.010.
[28] C.H. Wang, K. Sidhu, T. Yang, J. Zhang, R. Shanks, Interlayer self-healing and toughening of carbon fibre/epoxy composites using copolymer films, Compos. Part A Appl. Sci. Manuf. 43 (2012) 512–518, https://doi.org/10.1016/j.compositesa.2011.11.020.
[29] J. Lee, D. Bhattacharyya, M.Q. Zhang, Y.C. Yuan, Mechanical properties of a self-healing fibre reinforced epoxy composites, Compos. B Eng. 78 (2015) 515–519, https://doi.org/10.1016/j.compositesb.2015.04.014.
[30] A.R. Jones, C.A. Watkins, S.R. White, N.R. Sottos, Self-healing thermoplastic-toughened epoxy, Polymer 74 (2015) 254–261, https://doi.org/10.1016/j.polymer.2015.07.028.
[31] C.M. Dry, N.R. Sottos, Passive smart self-repair in polymer matrix composite materials, in: Conference on Recent Advances in Adaptive and Sensory Materials and Their Applications, Technomic, Virginia, USA, 1992, pp. 438–444.
[32] C. Dry, Procedures developed for self-repair of polymer matrix composite materials, Compos. Struct. 35 (1996) 263–269, https://doi.org/10.1016/0263-8223(96)00033-5.
[33] E.N. Brown, S.R. White, N.R. Sottos, Retardation and repair of fatigue cracks in a microcapsule toughened epoxy composite - Part I: manual infiltration, Compos. Sci. Technol. 65 (2005) 2466–2473, https://doi.org/10.1016/j.compscitech.2005.04.020.
[34] E.N. Brown, S.R. White, N.R. Sottos, Retardation and repair of fatigue cracks in a microcapsule toughened epoxy composite - Part II: in situ self-healing, Compos. Sci. Technol. 65 (2005) 2474–2480, https://doi.org/10.1016/j.compscitech.2005.04.053.
[35] J.D. Rule, N.R. Sottos, S.R. White, Effect of microcapsule size on the performance of self-healing polymers, Polymer 48 (2007) 3520–3529, https://doi.org/10.1016/j.polymer.2007.04.008.
[36] Y.T. Zhang, H.C. Yu, M.C. Shen, Y.T. Chern, C.C. Li, Synthesis and application of self-healing microcapsules containing curable glue, Mater. Chem. Phys. 240 (2020) 122161, https://doi.org/10.1016/j.matchemphys.2019.122161.
[37] T. Engel, G. Kickelbick, Self-healing nanocomposites from silica-polymer core-shell nanoparticles, Polym. Int. 63 (2014) 915–923, https://doi.org/10.1002/pi.4642.
[38] Y. Taguchi, N. Saito, K. Fuchigami, M. Tanaka, Preparation of hybrid microcapsules and application to self-healing agent, Polym. Adv. Technol. 25 (2014) 41–47, https://doi.org/10.1002/pat.3202.
[39] J. Lee, D. Bhattacharyya, M.Q. Zhang, Y.C. Yuan, Fracture behaviour of a self-healing microcapsule-loaded epoxy system, Express Polym. Lett. 5 (2011) 246–253, https://doi.org/10.3144/expresspolymlett.2011.24.
[40] M.G. Ahangari, A. Fereidoon, Micromechanical properties and morphologies of self-healing epoxy nanocomposites with microencapsulated healing agent, Mater. Chem. Phys. 151 (2015) 112–118, https://doi.org/10.1016/j.matchemphys.2014.11.044.
[41] M. Raimondo, P. Longo, A. Mariconda, L. Guadagno, Healing agent for the activation of selfhealing function at low temperature, Adv. Compos. Mater. 24 (6) (2015) 519–529.
[42] L. Guadagno, A. Mariconda, A. Agovino, M. Raimondo, P. Longo, Protection of graphene supported ROMP catalyst through polymeric globular shell in self-healing materials, Compos. B Eng. 116 (2017) 352–360.
[43] P. Longo, A. Mariconda, E. Calabrese, M. Raimondo, C. Naddeo, L. Vertuccio, S. Russo, G. Iannuzzo, L. Guadagno, J. Ind. Eng. Chem. 54 (2017) 234–251.
[44] R.S. Trask, I.P. Bond, Biomimetic self-healing of advanced composite structures using hollow glass fibres, Smart Mater. Struct. 15 (2006) 704–710, https://doi.org/10.1088/0964-1726/15/3/005.
[45] J.W.C. Pang, I.P. Bond, A hollow fibre reinforced polymer composite encompassing self-healing and enhanced damage visibility, Compos. Sci. Technol. 65 (2005) 1791–1799, https://doi.org/10.1016/j.compscitech.2005.03.008.
[46] S. Kling, T. Czigány, Damage detection and self-repair in hollow glass fiber fabric-reinforced epoxy composites via fiber filling, Compos. Sci. Technol. 99 (2014) 82–88, https://doi.org/10.1016/j.compscitech.2014.05.020.
[47] J. Sun, H. Li, C. Wang, D. Yuan, L.P. Stubbs, C. He, The effect of residual solvent N, N′-Dimethylformamide on the curing reaction and mechanical properties of epoxy and lignin epoxy composites, Macromol. Chem. Phys. 217 (2016) 1065–1073, https://doi.org/10.1002/macp.201500453.
[48] M. Tanimoto, S. Ando, Prevention of void formation in particulate-filled polymer composites: effects of thermoplastic matrices and residual solvent, Compos. Sci. Technol. 123 (2016) 268–275, https://doi.org/10.1016/j.compscitech.2015.12.022.
[49] J. Coates, Interpretation of infrared spectra, A practical approach, Encycl. Anal. Chem. (2006) 1–23, https://doi.org/10.1002/9780470027318.a5606.
[50] L. Guadagno, M. Raimondo, Use of FTIR analysis to control the self-healing functionality of epoxy resins, in: T. Theophile (Ed.), Infrared Spectroscopy Materials Science, Engineering and Technology, InTech, Croatia, 2012, pp. 285–300.
[51] H. Lee, A. Abarghani, B. Liu, M. Shokouhimehr, M. Ostadhassan, Molecular weight variations of kerogen during maturation with MALDI-TOF-MS, Fuel 269 (2020) 117452, https://doi.org/10.1016/j.fuel.2020.117452.
[52] B. Janković, N. Manić, I. Radović, M. Janković, M. Rajačić, Model-free and model-based kinetics of the combustion process of low rank coals with high ash contents using TGA-DTG-DTA-MS and FTIR techniques, Thermochim. Acta 679 (2019) 178337, https://doi.org/10.1016/j.tca.2019.178337.
[53] Y. Zhang, X. Chen, B. Zheng, X. Guo, Y. Pan, H. Chen, H. Li, S. Min, C. Guan, K. W. Huang, J. Zheng, Structural analysis of transient reaction intermediate in formic acid dehydrogenation catalysis using two-dimensional IR spectroscopy, Proc. Natl. Acad. Sci. U.S.A. 115 (2018) 12395–12400, https://doi.org/10.1073/pnas.1809342115.
[54] T. Sato, K. Kunimatsu, K. Okaya, H. Yano, M. Watanabe, H. Uchida, In situ ATR-FTIR analysis of the CO-tolerance mechanism on Pt 2Ru3/C catalysts prepared by the nanocapsule method, Energy Environ. Sci. 4 (2011) 433–438, https://doi.org/10.1039/c0ee00232a.
[55] C. Elmasides, D.I. Kondarides, S.G. Neophytides, X.E. Verykios, The oxidation state of Ru catalysts under conditions of partial oxidation of methane studied by XPS and FTIR spectroscopy, Stud. Surf. Sci. Catal. 130 (2000) 3083–3088, https://doi.org/10.1016/s0167-2991(00)80495-4.
[56] M.B. Dinger, J.C. Mol, Degradation of the second-generation Grubbs metathesis catalyst with primary alcohols and oxygen - isomerization and hydrogenation activities of monocarbonyl complexes, Eur. J. Inorg. Chem. (2003) 2827–2833, https://doi.org/10.1002/ejic.200200702.
[57] J.A. Martín, A. Solla, S. Woodward, L. Gil, Fourier transform-infrared spectroscopy as a new method for evaluating host resistance in the Dutch elm disease complex, Tree Physiol. 25 (2005) 1331–1338, https://doi.org/10.1093/treephys/25.10.1331.
[58] I.L. Schneider, E.C. Teixeira, D.M. Agudelo-Castañeda, G. Silva e Silva, N. Balzaretti, M.F. Braga, L.F.O. Silva, FTIR analysis and evaluation of carcinogenic and mutagenic risks of nitro-polycyclic aromatic hydrocarbons in PM1.0, Sci. Total Environ. 541 (2016) 1151–1160, https://doi.org/10.1016/j.scitotenv.2015.09.142.
[59] M.M. ElFaham, A.M. Mostafa, G.M. Nasr, Unmanned aerial vehicle (UAV) manufacturing materials: synthesis, spectroscopic characterization and dynamic mechanical analysis (DMA), J. Mol. Struct. 1201 (2020) 127211, https://doi.org/10.1016/j.molstruc.2019.127211.
[60] I. Oikonomopoulos, T. Perraki, N. Tougiannidis, Ftir study of two different lignite lithotypes from neocene achlada lignite deposits in nw Greece, Bull. Geol. Soc. Greece 43 (2017) 2284, https://doi.org/10.12681/bgsg.14312.
[61] M. Ashok, A.V.S.S. Prasad, V. Ravinder, Synthesis, spectral studies and catalytic activity of ruthenium(II) complexes with organic amide ligands, J. Braz. Chem. Soc. 18 (2007) 1492–1499, https://doi.org/10.1590/S0103-50532007000800007.
[62] H. Czichos, T. Saito, L. Smith, Springer Handbook of Materials Measurement Methods, Springer Berlin Heidelberg, 2006.
[63] R.A. Chowdhury, M.V. Hosur, M. Nuruddin, A. Tcherbi-Narteh, A. Kumar, V. Boddu, S. Jeelani, Self-healing epoxy composites: preparation, characterization and healing performance, J. Mater. Res. Technol. 4 (2015) 33–43, https://doi.org/10.1016/j.jmrt.2014.10.016.
[64] J.M. Lenhardt, S.H. Kim, A.J. Nelson, P. Singhal, T.F. Baumann, J.H. Satcher, Increasing the oxidative stability of poly(dicyclopentadiene) aerogels by hydrogenation, Polymer 54 (2013) 542–547, https://doi.org/10.1016/j.polymer.2012.12.002.
[65] D. Schaubroeck, S. Brughmans, C. Vercaemst, J. Schaubroeck, F. Verpoort, Qualitative FT-Raman investigation of the ring opening metathesis polymerization of dicyclopentadiene, J. Mol. Catal. A Chem. 254 (2006) 180–185, https://doi.org/10.1016/j.molcata.2006.01.074.
[66] S.E. Barnes, E.C. Brown, N. Corrigan, P.D. Coates, E. Harkin-Jones, H.G. M. Edwards, Raman spectroscopic studies of the cure of dicyclopentadiene (DCPD), Spectrochim. Acta Part A Mol. Biomol. Spectrosc. 61 (2005) 2946–2952, https://doi.org/10.1016/j.saa.2004.11.005.
[67] A. Della Martina, L. Garamszegi, J.G. Hilborn, Surface functionalization of cross-linked poly(dicyclopentadiene), React. Funct. Polym. 57 (2003) 49–55, https://doi.org/10.1016/j.reactfunctpolym.2003.07.003.
[68] J. Wonje, M.R. Kessler, Toughness enhancement in ROMP functionalized carbon nanotube/polydicyclopentadiene composites, Chem. Mater. 20 (2008) 7060–7068, https://doi.org/10.1021/cm8020947.
[69] T. Kevin O'Brien, Composite Materials: Fatigue and Fracture, Third Vol, ASTM, Philadelphia, 1991.